ANALYSIS OF INTERANNUAL VARIABILITY IN THE EASTERN EQUATORIAL PACIFIC OCEAN USING A HIGH RESOLUTION REGIONAL OCEAN MODELING SYSTEM

A Thesis

by

OTONIEL CESAR PALACIOS CELIN

Submitted to the Office of Graduate and Professional Studies of
Texas A&M University
in partial fulfillment of the requirements for the degree of

MASTER OF SCIENCE

Chair of Committee,	Benjamin Giese
Committee Members,	Robert Hetland
	Gerald North
Head of Department,	Debbie Thomas

May 2016

Major Subject: Oceanography

ABSTRACT

Interannual variability in the Eastern Equatorial Pacific Ocean is explored using a high resolution ocean model. The model domain covers the coast of South America to 96°W, including the Galapagos Islands, and from 15°S to 15°N. An experiment based on a run from January 1990 to December 1999 is conducted using the Simple Ocean Data Assimilation version sparse input.2 (SODAsi.2) 5 day data sets for the initial and boundary conditions. For surface forcing the 20CRV2 (20th Century Reanalysis version 2) daily data set is used.

The model results are compared with observations from a buoy that is part of the Tropical Atmosphere Ocean (TAO) project located at 95°W and over the equator, the model captures the main features of annual and interannual variability, although there are some notable discrepancies.

At the surface we can identify the most important features of the domain of study that are the equatorial cold tongue, the Costa Rica Dome and the east Pacific warm pool. In the subsurface the thermal distribution agrees with the typical behavior of the east Pacific Ocean such as strong stratification and a shallow thermocline.

The results show strong anomalies of sea surface temperature (SST) and sea surface height (SSH) during El Niño. Changes in conditions at the surface and subsurface demonstrate the strength of the 97-98 El Niño event, especially when compared with the weaker 1991-92 event. The results are also used to explore changes in circulation around the Galapagos during El Niño.

DEDICATION

I dedicate this thesis to my son Othoniel, my daughter Domenica, my mother Beatriz and the memory of my father Othoniel, my grandparents Jose and Carmen, and my wife Ingrid for their love, support and teaching during my life.

Specially, for my beautiful wife Ingrid, my daughter Domenica and my son Othoniel for their love dedicated every time.

ACKNOWLEDGMENTS

I would like to thank my committee chair, Dr. Benjamin Giese, and my committee members, Dr. Robert Hetland and Dr. Gerald North, for their guidance, support, and patience throughout the course that allows me to complete the research.

Thanks also go to Dr. Howard Seidel, who supports me in several aspects during my research.

Finally, thanks to my mother and wife for their encouragement, patience and love.

TABLE OF CONTENTS

LIST OF FIGURES

FIGURE Page

CHAPTER I

INTRODUCTION

1.1 Annual Variability and Seasonal Cycle

The eastern Tropical Pacific Ocean plays an important role in global climate variability and the interaction between ocean and atmosphere in the Pacific basin. Although the sun crosses the equator twice during a year, there is a strong annual harmonic that controls sea surface temperature (SST) variations in the eastern Tropical Pacific Ocean [*Li and Philander*, 1996]. Under normal conditions, SST has maximum values during the northern spring due to the relaxation of the southeast trade winds [*Philander*, 1981]. By contrast, minimum SST values occur during the northern summer and autumn when the easterly trade winds intensify. As a result, there is a curious asymmetry that arises with the cycle of winds and SST out of phase with solar forcing during autumnal equinox, the southeast trades are intense and the northeast trades decrease in intensity; but during the vernal equinox there is a relaxation of the easterly tradewinds. Similarly, SST influences the position of the Inter Tropical Converge Zone (ITCZ) due to changes in heat flux across the surface of the ocean [*Philander*, 1981; *Li and Philander*, 1996; Philander et al., 1996], this heat flux consist on net radiation (short minus long wave) and evaporation at the ocean surface. As a consequence of the ITCZ variation, the wind stress pattern is influenced by the seasonal cycle of SST. Therefore, there is a feedback between ocean and atmosphere in the tropical areas [*Bjerkens*, 1969; *Xie*, 1994] that is positive according to Bjerknes when normal conditions occur.

Seasonal variation of surface winds in the eastern Equatorial Pacific involves changes of equatorial upwelling and thermocline depth. During the period of intense southeast trades, coastal equatorial upwelling is induced at the coasts of Peru and Ecuador that spreads a tongue of cold surface waters from east to west to approximately 100°W during Northern Hemisphere summer and autumn. As a result, during a normal year warm water is displaced toward the north after August. On the other hand, the upwelling is reduced when the easterly tradewinds weaken during spring. Intensified upwelling arises between September and October as a combination of zonal advection, meridional diffusion and vertical entrainment [*Kessler*, 2006]. In addition, surface equatorial ocean circulation is also affected by the weakening of easterlies, resulting in a weakening of the North Equatorial Countercurrent. Interestingly this is also the time when the speed of the Equatorial Undercurrent reaches its maximum [*Philander*, 1981]. Moreover, the thermocline in the eastern Equatorial Pacific is normally shallow because the advection of westward trade winds that maintain the warm surface waters in the western Tropical Pacific, hence the surface to the east is exposed to cold water. In the equatorial plane, there is a balance between the eastward pressure force, related to the slope of the thermocline and westward wind stress. This balance is disturbed by the relaxation of the trade winds. In this case, the thermocline deepens in the east, and rises in the western side of the Equatorial Pacific Ocean, a hallmark of changes that occur during the El Niño Southern Oscillation (ENSO).

1.2 Interannual Variability and El Niño

There are similarities in the response of the tropical Pacific Ocean to interannual and seasonal wind variations. For instance, SST values are high in the Eastern Tropical Pacific when southeast trades decrease in intensity at both seasonal and interannual timescales. However, the magnitude of the interannual zonal redistribution of warm sea surface water is greater in comparison with the seasonal distribution of warm water because interannual changes depend on large-scale processes [*Li and Philander*, 1996]. A pronounced change in the temperature of the water column due to internannual warming involves deepening of the thermocline, thus there is an increase in the sea level when this process happens, so that there is a positive correlation between thermocline depth and sea level. The most prominent interannual variability across the tropical Pacific Ocean is related to the occurrence of El Niño and La Niña [*Jin and Neelin*, 1993; *Giese and Carton*, 1999; *Russon et al.*, 2014].

ENSO event has a recurrence at irregular intervals between 2-7 years with significant changes in the ocean and atmosphere of the tropical Pacific Ocean that influences other regions. The oceanographic component is called El Niño, and atmospheric changes are termed the Southern Oscillation. El Niño got its name from Peruvian fishermen because warming often appears after Christmas [*Wyrtki*, 1975; *Rasmusson and Carpenter*, 1982]. When El Niño arises there is an unusual warming of SST in the eastern equatorial Pacific accompanied by a weakening of easterlies close to the equator. Equatorial upwelling is reduced, thus the cold tongue recedes [*Xie*, 1994; *Russon et al*., 2014]. Because of the imbalance between the zonal wind variation and the

eastward pressure force in the equatorial Pacific region, westerly wind anomalies induce a transport of warm water eastward. Thus, there is a pronounced deepening of the thermocline in the eastern side with a concomitant rise of sea level. The interannual El Niño event represents the negative phase of the feedback between ocean and atmosphere described by Bjerknes [1969] related to the weakening of the Walker circulation.

El Niño evolution has a strong relationship with the annual cycle of the eastern Tropical Pacific. El Niño usually grows during boreal summer and fall and reaches a warming peak in the middle of northern winter, which gives rise to a "phase-locking" of El Niño to the seasonal cycle [*Sarachik and Cane*, 2010]. *Rasmusson and Carpenter* [1982] suggested that between the years 1949 and 1976 the peak of SST anomalies along Ecuador and Peru occurred during boreal spring of the year of development of El Niño (El Niño year). In contrast, *Wang* [1995] shows that during 1977 and 1996 the warming peak along South American coasts was in the boreal spring subsequent to El Niño year. El Niño of 1997-1998 presents a peculiar development with a strong amplification in the central Pacific and along the coast of South America during spring of 1997 [*Wang and Weisberg*, 2000; *Wang and Fiedler*, 2006]. In summary, several studies suggest that seasonal cycle of the eastern Equatorial Pacific plays an important role in the evolution and dynamics of El Niño, and maybe even the probable reason for El Niño irregularity [*Tziperman et al*., 1994; *Chang* , 1993; *Tziperman et al*., 1997].

1.3 Numerical and Interannual Variability Studies

During the last few years, there were important efforts to improve the systems observations of the oceans in order to better understand the main processes that occur in the surface and subsurface tropical Pacific Ocean. However, the information obtained from buoys and satellites is limited in time and in space [*Colas et al*., 2008; *Montes et al*., 2010]. One consequence of these limited observations is mesoscale process, for example eddies, that the role is not known. Satellite information represents only a view of the surface of the ocean with a limited view of the subsurface. In addition, several studies of the dynamics of the Eastern Tropical Pacific are based on the use of Ocean General Circulation Models (OGCMs) [*Kessler et al*., 2006; *Montes et al*., 2010]. For example, *Philander et al.* [1987], *Li and Philander* [1995], and *Kessler et al.* [1997] suggest that there are pronounced changes in the seasonal cycle of variables such as SST, surface winds, and cloudiness. Nevertheless, OGCMs typically have a resolution that does not resolve mesoscale variability. This effort addresses the need to better understand this variability.

Recently, high resolution primitive-equation models have been used to focus understand the seasonal cycle and interannual variability in the eastern Tropical Pacific [*Penven et al*., 2005; *Colas et. al*, 2008; *Dewitte et al*., 2012]. *Penven et al.* [2005] was able to accurately reproduce the average circulation of the Peru Current System using the Regional Ocean Modeling System (ROMS), but with a bias in SST. They suggests that the upwelling presents a strong influence on the seasonal cycle of SST by considering both local and remote forcing. Despite the bias in SST, the model of *Penven et al.* [2005] was

able to represent the main features of eastern Pacific circulation, for example the dynamics of the equatorial cold tongue.

The 1997-1998 El Niño was reproduced by *Colas et al.* [2008] in a high resolution model. This study confirmed the delayed recovery from ENSO conditions after the second peak of the phenomenon in 1998. Moreover, they showed that the intensity of equatorial coastal upwelling is governed by wind intensity and poleward advection that involves the flow of the coastal trapped waves, and cross-shore geostrophic flows. *Montes et al.* [2010] presents a study of the circulation of eastern Equatorial Pacific focusing on equatorial, and coastal upwelling and the effect of eddies in the mesoscale variability. It is important to consider that the studies during the last decade using a high resolution ROMS model on this area were concentrated in the understanding of changes and mean circulation of the coastal upwelling of Peru and the circulation of the Peru Current system. The present study is focusing on observing and diagraming the eastern Equatorial Pacific along the Equator involving the area around Galapagos Islands.

CHAPTER II

DATA AND METHODOLOGY

2.1 Model Characteristics

A high resolution Regional Ocean Modeling System (ROMS) Rutgers version 3.7 is used to explore annual and interannual variability in the Eastern Tropical Pacific. A complete description of the model is given by *Haidvogel et al.* [2000, 2008], and *Shchepetkin and McWilliams* [2003, 2005]. Here we briefly describe the most relevant details related to our version of the model. ROMS is a three-dimensional, free surface, terrain-following, curvilinear coordinate model that solves the primitive equations using the hydrostatic and Boussinesq approximations [*Haidvogel et al*., 2000; *Marshesiello et al*., 2001; *Penven et al*., 2005, *Lemarie et al*., 2012]. Under the hydrostatic approximation, the vertical pressure gradient balances the buoyancy force. The Boussinesq approximation ignores variations in density in the momentum equations, however, changes in density are kept in the vertical momentum equations due to buoyancy forcing.

The terrain-following vertical (sigma) coordinates are used to discretize the primitive equations over variable topography [Song and *Haidvogel*, 1994]. The theory of sigma coordinates was introduced by *Phillips* [1957] in atmospheric modeling. In the physical domain of the ocean, the most used vertical coordinate is the z-coordinate (meters). However, in numerical ocean modeling there are problems representing variations in the topography of the ocean, mainly near coastal boundaries due to the difficulty of treating the bottom kinematic stress boundary conditions and horizontal

mixing of momentum [*Song and Haidvogel*, 1994]. In contrast, sigma coordinates follow the bathymetry of the ocean and simplifies the computation of the model. The reason is because sigma coordinates transform the irregular physical topography of the ocean to a fixed regular computational domain. Sigma coordinates are able to provide an enhanced vertical resolution depending on the area of interest, such as above the thermocline or close to the bottom of the ocean.

A sigma value represents the vertical distance from the surface measured as a fraction of the local water column thickness through the following relationship: $-1 \leq \text{sigma } 0 \leq 1$, where -1 corresponds to the sea floor and sigma = 0 corresponds to the sea surface according to *Shchepetkin and McWilliams* [2003]. Past studies reveal that there is strong topographic sensitivity of the model using sigma coordinates that involves pressure gradient errors due to the intersection of the vertical coordinate with the isopycnals [*Shchepetkin and McWilliams*, 2005]. There are corrections in the numerical algorithms of the model in order to reduce these errors.

A split-explicit time-stepping scheme is implemented in ROMS model to solve the hydrostatic primitive equations for momentum in order to improve the computational efficiency. This process involves a coupling between barotropic and baroclinic time steps. A specific number of fast batrotropic time steps are computed within each baroclinic time step in order to integrate the model. The barotropic fields are averaged in time to be used with the larger baroclinic time steps. This calculation avoids noise in the frequencies unresolved by baroclinic steps.

2.2 Model Setup

The model curvilinear grid covers the Eastern Equatorial Pacific from the coast of South America to 100°W, and includes the Galapagos Islands, and from 15°S to 15°N. The horizontal resolution varies from 7.5 km and 9.5 km. This high resolution allows the resolve of mesoscale process features, for instance eddies and the Costa Rica Dome [*Penven et al*., 2005; *Colas et al*., 2008]. The horizontal grid contains 330 x 280 points. The bottom topography in calculated from etopo1 with a resolution of 1 arc minute, with a factor related to topographic slope (r-factor) of 0.25. The model has 30 vertical levels, the vertical stretching parameters are: theta s =5.0, theta b=0.1, with a critical depth of 200 meters according to the formulation of *Song and Haidvogel* [1994] and the configuration of *Colas et al.* [2008]. This configuration gives more resolution near the surface because we will be analyzing the upper layers of the open ocean; coastal processes that require high resolution near the bottom are not considered in this study.

The model has open boundary conditions on the western and southern sides, the northern and western boundaries are closed with no-slip boundary conditions. At the open boundaries a Chapman scheme [*Chapman*, 1985] is employed for free surface elevation, a Flather scheme [*Flather*, 1976] is used for the 2-D momentum equations, and a combination of radiation and nudging schemes are used for the 3-D momentum equations and tracers that include temperature and salinity. We specify the nudging values with a nudging timescale of 30 days for outflow and one day for active conditions or inflow. This nudging timescale configuration allows us to detect the main changes in the seasonal cycle of SST (Figure 1) for the entire period of the run, between 1990 and 1999. The warmest

period occurs in 1997-1998 associated with the strong El Niño. Figure 2 shows changes in the zonal component of wind stress. The barotropic time step is set to 10 seconds and the baroclinic time step is 150 seconds. The model is parameterized with a third-order bias advection scheme in order to discretize the horizontal momentum, with a logarithmic bottom friction of momentum, and harmonic mixing of momentum. The turbulence closure is parameterized with a Mellor-Yamada 2.5 scheme [*Mellor and Yamada*, 1982].

A ROMS model run from January 1990 to December 1999 is computed using the Simple Ocean Data Assimilation version sparse input.2 (SODAsi.2) 5 day data set for the initial and boundary conditions. Surface forcing is from the 20CRV2 (20^{th} Century Reanalysis version 2) [*Whitaker et al*., 2004; *Compo et al*., 2006; *Compo et al*., 2011] daily data set. The model has a spinup of four years from January 1986 to December 1989.

2.3 SODAsi.2 Data Set

SODAsi.2 is a new ocean reanalysis data set that spans the period from 1845 to 2011 [*Giese et al*., in preparation]. This new version of SODA reanalysis follows the methodology used in several old versions of SODA that cover the 20^{th} Century. The main difference is that SODAsi.2 is based on an ensemble of reanalysis forcing fields instead of using the ensemble mean of an atmospheric reanalysis. This improvement avoids biases related to sparse observations in earlier years of the century. The SODA system was developed using the Parallel Ocean Program (POP) [*Smith et al*., 1992] ocean model and SODA algorithm.

The POP model is an Ocean General Circulation Model with an average horizontal resolution of 0.25° x 0.4° with 40 vertical levels, and 10 meters spacing in the 100 m below the ocean surface [*Carton and Giese*, 2008; *Giese and Ray*, 2011] . The model has a global domain and uses a displaced pole in order to resolve Arctic processes. Poleward of the equator there is an increase in the meridional resolution to reduce the grid anisotropy as a result of the use of the Mercator coordinate system. Bottom topography comes from the 1/30 analysis of Smith and Sandwell [*Carton and Giese*, 2008]. Vertical diffusion uses the K-profile parameterization (KPP) mixing, and biharmonic mixing is employed for lateral subgrid-scale processes (horizontal mixing).

Data assimilation includes only SST observations from ICOADS 2.5 (International Comprehensive Ocean-Atmosphere data set version 2.5) and is carried out using a sequential 10-day update cycle. A simulation without assimilation is used to obtain the model error covariance. The SODA cycle is as follows. The ocean model is integrated forward for 5 days to produces estimates of temperature and salinity. The difference between the analysis and the first guess is used to calculate innovations. The ocean model is restarted at day t and calculated to t+10 with temperature and salinity innovations added at each time step. The procedure is repeated at day t+10. The output variables of the model are recorded with 5 days averaged mapped on an uniform global 0.5° x 0.5° (720x330x40 points) horizontal grid through the horizontal grid spherical coordinate remapping and an interpolation package from *Jones* [1999]. For surface boundary conditions for the ocean model 18 out of 56 ensemble members from C20Rv2 were chosen. Surface momentum fluxes are calculated from surface wind stress of C20Rv2. Heat and fresh water fluxes

come from computing solar radiation, specific humidity, cloud cover, 2m temperature, precipitation, and 10 m wind stress using bulk formula.

2.4 C20Rv2 Data Set

20CRv2 is a reanalysis data set that provides information from the entire troposphere that covers the period from the middle of the nineteenth century until 2012. A coupled land-atmosphere model based on the NCEP Global Forecast System (GFS) is used for the 20CRv2 reanalysis. This model has a horizontal resolution of 200-km on an irregular Gaussian grid that is related to 62 spectral wavenumbers (T62) and a vertical resolution of 28 vertical hybrid sigma-pressure levels. Output is available every six hours. Boundary conditions of SST and sea ice concentration for 20CRv2 come from the UK Met Office HadISST1.1 data set. This data is interpolated in order to obtain a daily resolution. Surface pressure observations and Sea Level Pressure (SLP) are provided by the International Surface Pressure Databank (ISPD) [*Yin et al*., 2008] ICOADS [*Woodruff et al*., 2011] and the International Best Track Archive for Climatic Stewardship (IBTrACS) [*Kruk et al*., 2010]. Surface pressure observations involve information from land stations, marine observations, and tropical cyclone 'best track' pressure observations. SLP information is incorporated to the model from IOCADS 2.4 and 2.5. Data set from tropical cyclones are given by IBTrACS.

2.5 Comparison with Observational Data

A buoy that is part of the Tropical Atmosphere Ocean (TAO) project, located at 95°W at the equator, will be used to compare with ROMS output in order to demonstrate that ROMS is able to capture the main changes in temperature in a timescale realistically.

CHAPTER III

RESULTS

3.1 Comparison of ROMS Results with TAO Data

In situ temperature data from a buoy that is part of the Tropical Atmosphere Ocean (TAO) project is used in this study to compare the results of ROMS model with observational data. A vertical profile temperature of TAO buoy located at 95°W at the equator is used to estimate the ability of the ROMS model output to capture main features of interannual variability. The period of the study was chosen from March-01-1995 to July-31-1998, because there are extended gaps in data collected by the TAO buoy before and after this time. In addition, this time includes the most prominent change in interannual variability of the period of this study in the eastern Equatorial Pacific due to the El Niño 1997-1998.

Daily values of temperature from the TAO buoy data were binned into 5 day averages in order to compare with the ROMS output. Figure 1 shows the comparison of temperature between TAO and ROMS. As we can see, observed peaks of warm temperature are captured by ROMS during the years of comparison. The model temperature also captures the basic changes related to the annual cycle, thus we have warm episodes between February and the beginning of May each year, and cold episodes that peak in August and September. There is a general bias in the representation of the values in the cold phase of each year with values that are higher than expected in these months by about 1 to 1.5°C.

Changes in depth in TAO and ROMS are observed in figures 1a and 1b respectively. Annual variability in ROMS is well-defined in depth with a deepening of the thermocline during February and April and shoaling of the thermocline starting in August. Interannual variability in ROMS captures the warm phase of El Niño 1997-1998 with a peak of temperature below the surface between January and March in 1998. However, ROMS show a bias in the representation of the depth of thermocline mainly during January 1998 when temperature in TAO buoy reaches a maxima in depth, as a result we can observe that the thermocline deepens to a depth of 120 meters. The stratification below the mixed layer in ROMS shows an interannual change if we consider the difference between 1998 and 1996-1997 periods that give us an idea of the occurrence of a warm phase such as El Niño, but it is underestimated in comparison with TAO data. The evolution in time of the output of ROMS allows us to detect the main changes of annual to interannual variability where the most relevant bias is about the depth of the thermocline.

The El Niño 1997-1998 as represented by ROMS follows the typical sequence of ENSO with two peaks in SST to the west of the Galapagos Islands at the position of the TAO buoy (95°W) giving temperatures warmer than expected between August and October and with a peak in SST around March and April. However, there is a general negative bias in the representation of SST of about 1-1.5°C from February 1997 to May 1998. The SST modeled is about 29°C on the second peak of SST, but in TAO buoys, this value is about 30°C. Despite the bias in the values of SST is evident that in 1997-1998

there is a warmer event than the earlier years with a strong peak in 1998. Therefore, there is a bias in the sharp of the warm phases but not in the occurrence.

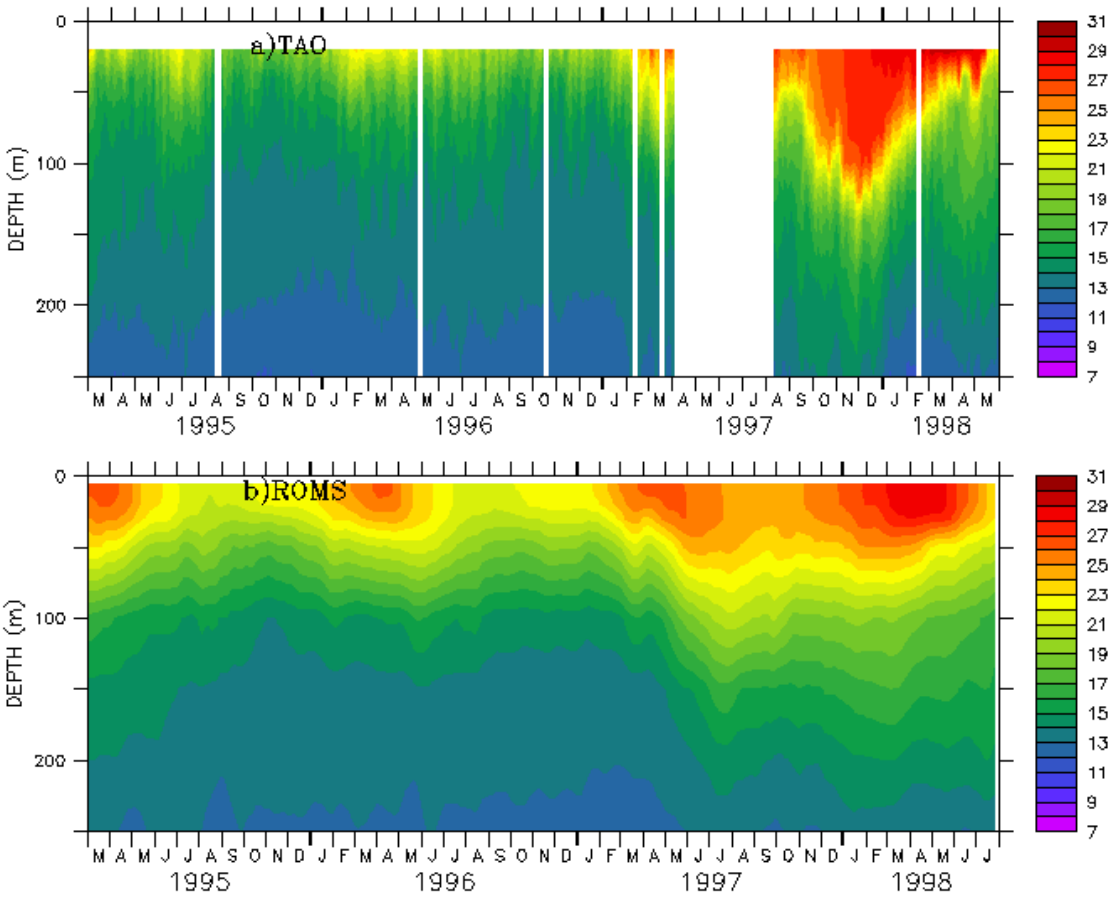

Figure 1. Comparison of TAO (a) with ROMS (b) for temperature (°C). (c) SST from TAO (black line) and ROMS (red line).

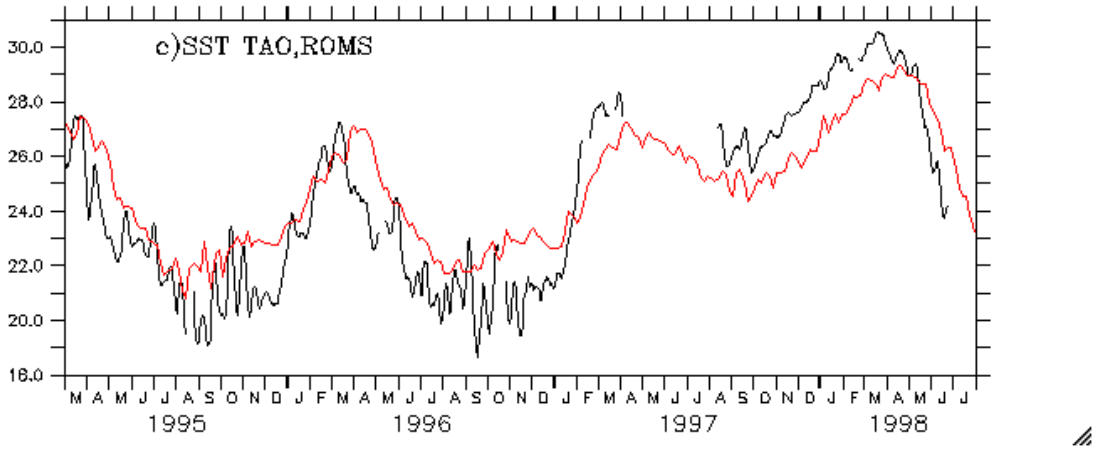

Figure 1. Continued.

3.2 Mean Conditions

3.2.1 Mean Surface Conditions

Sea surface temperature (SST) and surface velocity from the ROMS output averaged over 5 days were used to determine the mean surface conditions for the eastern Equatorial Pacific. The general features of the eastern Tropical Pacific are defined by the pattern of SST as shown in Figure 2. There is coastal upwelling off the Peru coast with its respective extension to the cold tongue of surface waters westward south the equator until 89°W. SST in the cold tongue has an oscillation between 23°C and 24°C according to the averaged values reproduced by ROMS in the Figure 2. This is the cold tongue that reach the eastern side of the Galapagos Islands during September-October under normal conditions.

The cold tongue is separated by a front with a moderate meridional gradient of SST that is located north of the equator. The position of this front depends on the location of the ITCZ. As we can observe in Figure 2, the mean meridional gradients of SST are

larger than those of the zonal gradients, except close to the coast of Peru that are influenced by the south-easterly winds. In general, the zonal component of wind is from east to west over the ITCZ domain. The mean SST of coastal upwelling in Figure 2 has values about 23°C.

The Costa Rica Dome and the eastern Pacific warm pool are well represented in modeled SST. The Costa Rica Dome, a feature caused by oceanic upwelling, is centered at 9°N, 80°W with an SST average of 25°C that agrees with the observed position of this feature. At the north-west side of the domain is a clearly defined warm pool with temperature above 27°C.

The mean surface zonal circulation is represented at 95°W by the currents as shown in Figure 2. Overall, the model is able to capture the main currents in the zone of study. South of 4°N in a wide band there is a westward current, the South Equatorial Current (SEC), with values around 60 cm s^{-1}. There is another westward current detected in the model that is the North Equatorial Current (NEC) located in a broad band north of 10°N. The NEC has a speed of 40 cm s^{-1}. This value is weak in comparison with the SEC. Between the NEC and SEC at approximately 5°N and 9°N, there is a prominent eastward current that flows with surface velocities of 50 cm/sec, this narrow current is the North Equatorial Countercurrent (NECC).

It is clear that westward currents transport cold ocean water, and eastward currents transport warm water. Therefore, there is a strong influence of advection in the process of warming and cooling in the region. In addition, the Peru current presents in the south-east boundary of the domain, brings cool water north because of coastal upwelling. Because of

the Peru current follows the mean circulation of winds, this current should strongly depend on changes of the wind. Consequently, we can anticipate that the position of the cold tongue will be impacted by changes in the easterlies.

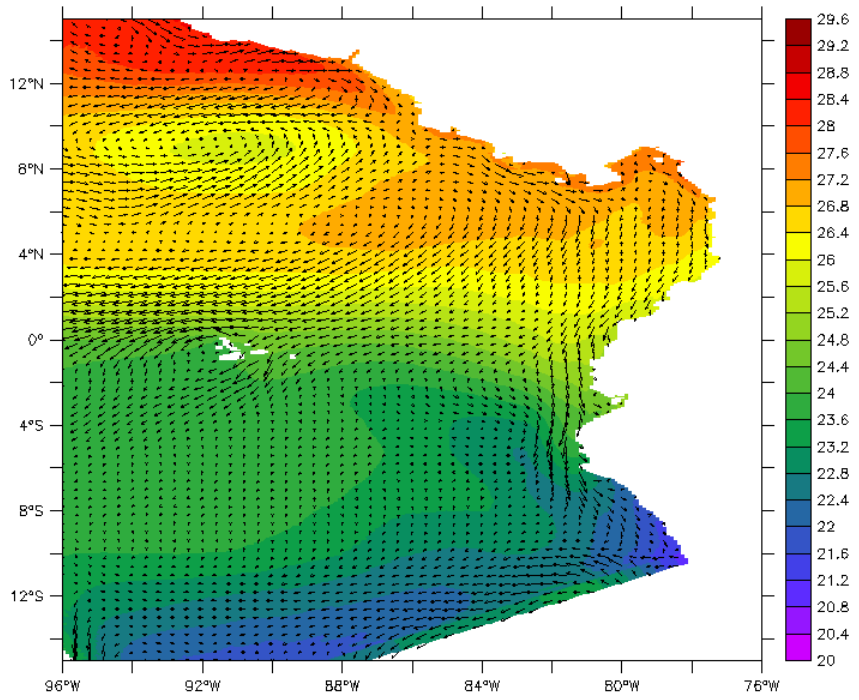

Figure 2. Sea surface temperature (°C) and surface circulation (m s^{-1}) for the period from 1990 to 1999.

3.2.2 Mean Vertical Structure

A mean vertical section of temperature along the equator between 96°W and the coast of the eastern equatorial Pacific is presented in Figure 3. It is noticeable that there is a strong subsurface thermal gradient that is close to the sea surface. This gradient is the

thermocline that is shallow at the eastern equatorial Pacific with a depth, shown in Figure 3, of around 50-60 meters. This shallow shoal thermocline divides the warm surface waters and the colder waters at depth. The mixed layer depth is about 30 meters with a temperature of about 25°C. Temperature decrease as a function of depth until about 100 meters where the temperature is 17-16°C. This gives an overall stratification of 1°C each 8 meters. This thin mixed layer makes SST sensitive to small changes of currents.

There is a stronger subsurface stratification on the eastern side of the Galapagos Island (90°W) in comparison with the western side. This change in the stratification is because the thermocline depth along the equator in the Pacific Ocean decrease from west to east. However, at first glance it is not obvious because just we are considering the eastern side of the region not the western equatorial Pacific, here we could find typically a thermocline depth of 150 meters. In Figure 3 the most prominent vertical thermal gradient is between 88°W and 82°W close to the coast of Ecuador.

The abrupt change in topography related to the position of the Galapagos Islands is remarkable in the vertical thermal structure showed in Figure 3, in the same way it is observed close to the coast at 82°W, where there is the influence of the coastal equatorial upwelling. The mean zonal section along the Equator in ROMS agrees well with the observed conditions in the region of study.

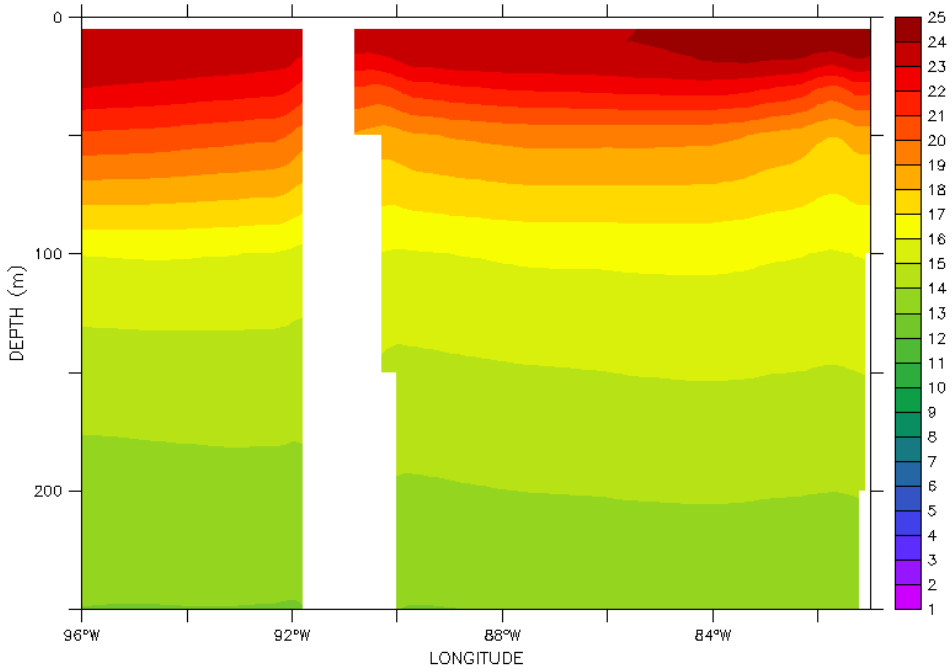

Figure 3. Mean vertical thermal structure (°C) at the equator.

A view of the model mean meridional section along 95°W shows the main subsurface circulation in Figure 4. Here we can observe the displacement of the Equatorial Under current (ECU) in the direction from west to east at a depth of about 60 meters until a depth of about 120-150 meters. The undercurrent rises over the west side of the Galapagos Islands, as a result there is coastal topographic upwelling in this region. This natural barrier causes that EUC to divide in two zonal eastward branches. The model is able to represent with certain realism the most relevant equatorial feature at the first's layer from the surface at the western of the Galapagos Islands.

Moreover, the South Equatorial current (SEC) in a westward direction is observed with the highest speed close to the surface. This current can be observed on both sides north and south of the equator. The strong part of the SEC is located north of the equator

at 4°N. From 5°N to 9°N, near to the surface, appears the North Equatorial Counter current (NECC). The strongest part of this current is located at 7°N. A branch of the North Equatorial current (eastward direction) is centered at 12°N.

Because geostrophy requires the currents in balance with density there is a correspondingly pattern of temperature. The isotherms of the North Equatorial Countercurrent (Figure 5) has a prominent slope from the deep ocean to the base of the mixed layer, as we can observe between 4°N and 8°N. In contrast, between 9°N and 14°N the slope of isotherms associated with the North Equatorial current is downward. It is clear from Figure 5 that the stratification of the thermocline starts to spread mainly in the south area at approximately 12°S. This spreading occurs due to the geostrophic balance between westward surface currents and the eastward Equatorial Undercurrent. This balance depends on the geostrophic meridional momentum equation, even near to the equator where the Coriolis parameter is close to zero,

Values of the subsurface currents near the equator are in the range of 0.2 - 0.6 m s^{-1}. The EUC has the highest value of about 0.5 m s^{-1} at a depth of 40 meters. Near to the surface the NECC has values about 0.4-0.7 m s^{-1}. The change in the current direction just to the northwest side of the Costa Rica Dome is located at about 11°N and 13°N. In the same area, it is observed that part of the extension in depth of the warm pool with temperatures of 27°C contrast with the values near the equator at about 25°C (Figure 5). It seems that the mixed layer is slightly deeper close to the warm pool of the Eastern Pacific in comparison with the equatorial region. In addition, strong thermal gradients are

found in the North Equatorial Countercurrent and the North Equatorial current respectively.

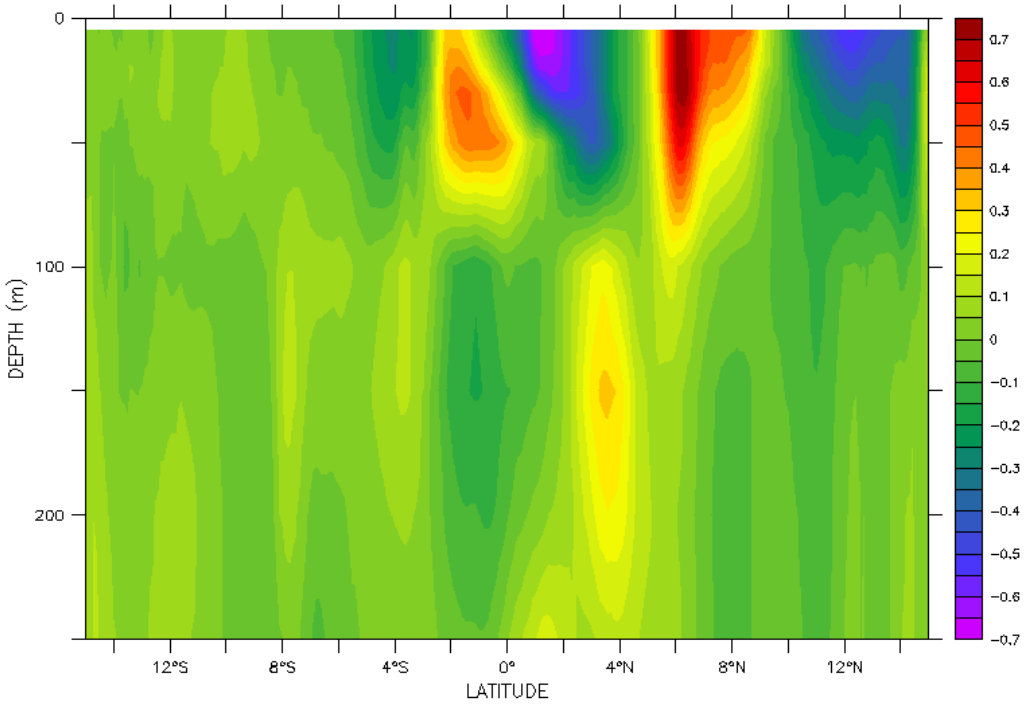

Figure 4. Model mean meridional section along 95°W of the subsurface circulation (m s^{-1}).

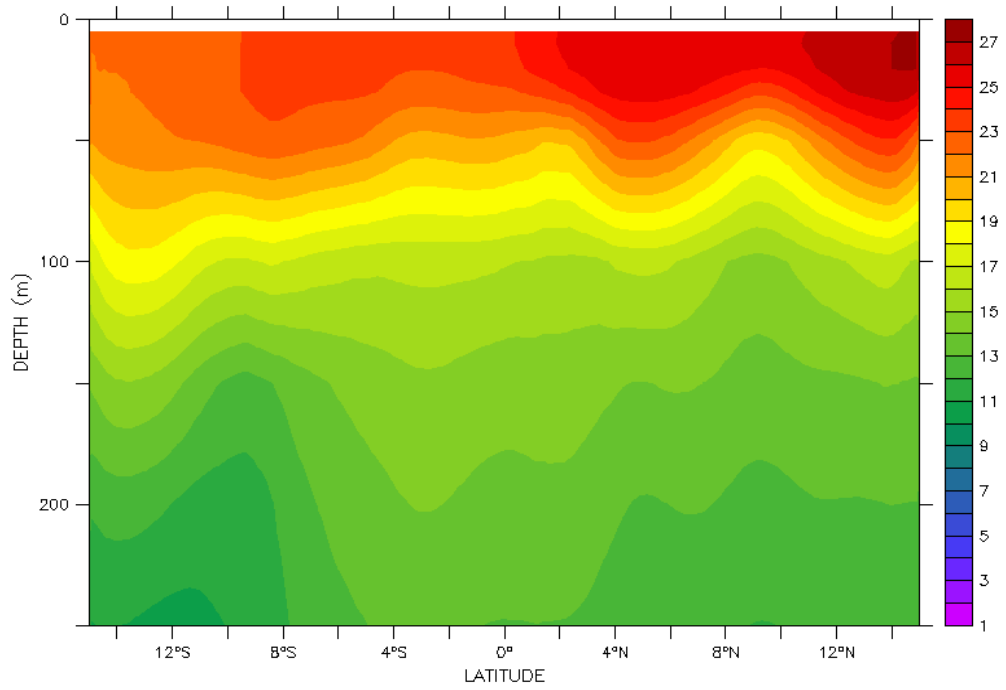

Figure 5. Model mean meridional section along 95°W of the thermal structure (°C).

3.3 Changes in ENSO Variability

3.3.1 Changes in SST

The variation in SST from ROMS output at the equator in the eastern Equatorial Pacific during the period between 1990 and 1999 is shown in Figure 6. As we can observe, the annual change shows a period of warm SST that rises recurrently at the beginning of each year. The peaks of temperature normally are between March and May with temperature variations that oscillates between 26°C and 29°C. The most noticeable peak is attained in 1998 and is related to the El Niño in that year. The lower temperatures occur between August and September with a variation in temperatures between 19°C and 25°C. Note that the coldest values are located at the western side of the Galapagos Islands. This

area is affected by the occurrence of coastal upwelling that generate cold surface temperatures.

Interannual variability related to El Niño is better seen by using SST model anomalies (Figure 7) that show the anomalies during the 1991-1992 and 1997-1998 events. Starting in July 1991 there are positive SST anomalies of 0.4°C, this coincides with the growing phase of El Niño. The mature phase and the corresponding positive anomalies of SST are apparent during the first part of 1992. The largest anomalies of the ten years of study occurs during El Niño of 1997-1998 between August 1997 and August 1998. It is noticeable that there is a first peak at the beginning of August 1997 and a second peak at the end of December 1997 beginning of 1998. The event terminate with a relaxation during April 1998. Consequently, neutral and negative anomalies are detected during September and October 1998 after the end of El Niño. There is a significant difference in the positive anomalies between El Niño 1991-1992 and El Niño 1997-1998 that is about 2°C to 3°C. El Niño 1991-1992 is considered a moderate event, thus the El Niño1997-1998 is considered a strong event.

Comparing the annual with the interannual distribution of SST in a time scale during the 10 years of study shows that there is a larger interannual variation of SST. This is observable in the event of El Niño 1992-1993 where the warm temperature is distributed in several months, but in the El Niño 1997-1998 is better observable the distribution of SST (Figure 6 and 7).

There is also annual and interannual responses the ocean to wind variations. The increasing of SST is associated with a period of relaxation of westward winds in the

eastern Tropical Pacific comparing modeled SST with the zonal wind stress variation from 1990 to 1999. Figure 8 shows the zonal wind stress component where there is a marked eastward movement during the first months of the year from January to April. After that there is an increase of the westward component just west of the Galapagos Islands. The region between 84° W and 82°W is affected by the topography of the coast of Peru that allows a considerable local eastward component that increases in intensity with the rise of southeast tradeswinds. Therefore, there is a defined annual cycle of the wind stress pattern in the eastern Equatorial Pacific.

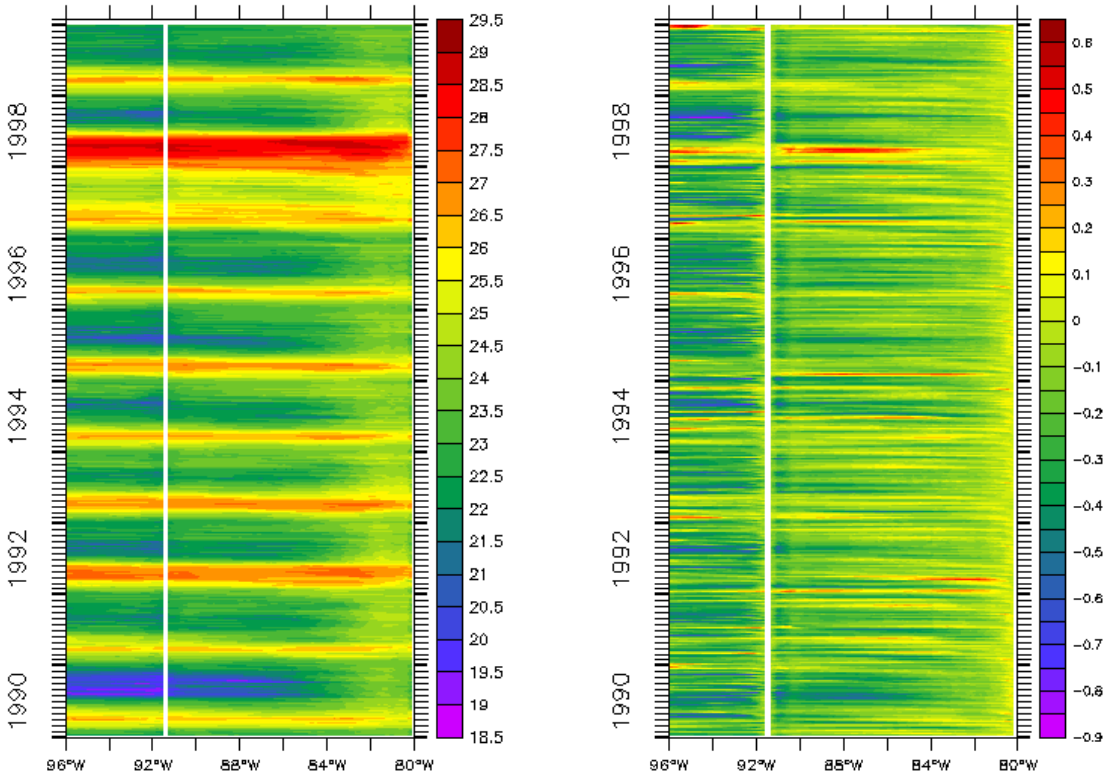

Figure 6. Time variation of SST (°C) and surface zonal velocity (m s^{-1}) at the equator.

Interannually the zonal wind stress has changes that are observable during El Niño (Figure 8). The zonal component of the wind stress near the coast is reduced in intensity during El Niño 1991-1992. In the El Niño 1997-1998 this component is reduced during August and September, after that the zonal component disappeared until the end of El Niño. Considering the relationship between equatorial upwelling and the intensity of winds at the eastern boundary of the Equatorial Pacific Ocean, we can infer that the reduction of windstress component close to the coast of Ecuador is directly associated with the reduction of the coastal equatorial upwelling.

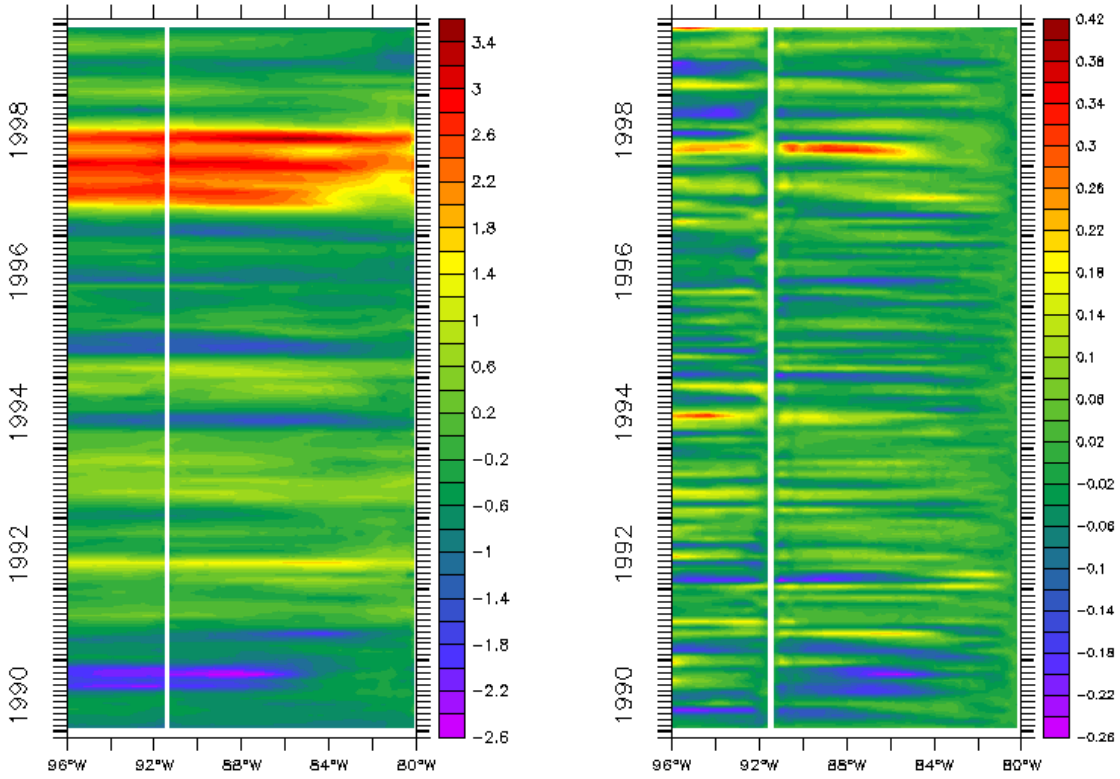

Figure 7. Time variation of SST (°C) anomalies and surface zonal velocity anomalies (m s^{-1}) at the equator.

3.3.2 Changes in SSH

The simulated sea surface height (SSH) for the period of study shows a marked annual oscillation. SSH reaches minimum values during August and September (Figure 9), and maximum values are observed during the first moths of the year, except for 1997 when SSH remains high for the entire year. The variation of SSH appears to be progressive and sustained during at least two or three weeks. However, there are some episodes of sharp changes detected in different years, typically after December.

The most important interannual change observed is during the occurrence of the 1997-1998 El Niño, when SSH maintains positive anomalies for most of the year in 1997 (Figure 9). There is a first peak that occurs in July, however the second peak in December is weaker than expected. During 1998 the highest value observed is at the end of February. During the El Niño of 1991-1992 the highest values are observed in 1992 in the second week of January. Despite the fact that the transition from positive to negative anomalies is strong, the transition from El Niño conditions to neutral conditions is slow and occurs after May in 1998 (Figure 9). Although is not clearly perceptible, SSH is slightly higher on the western side of the Galapagos Islands.

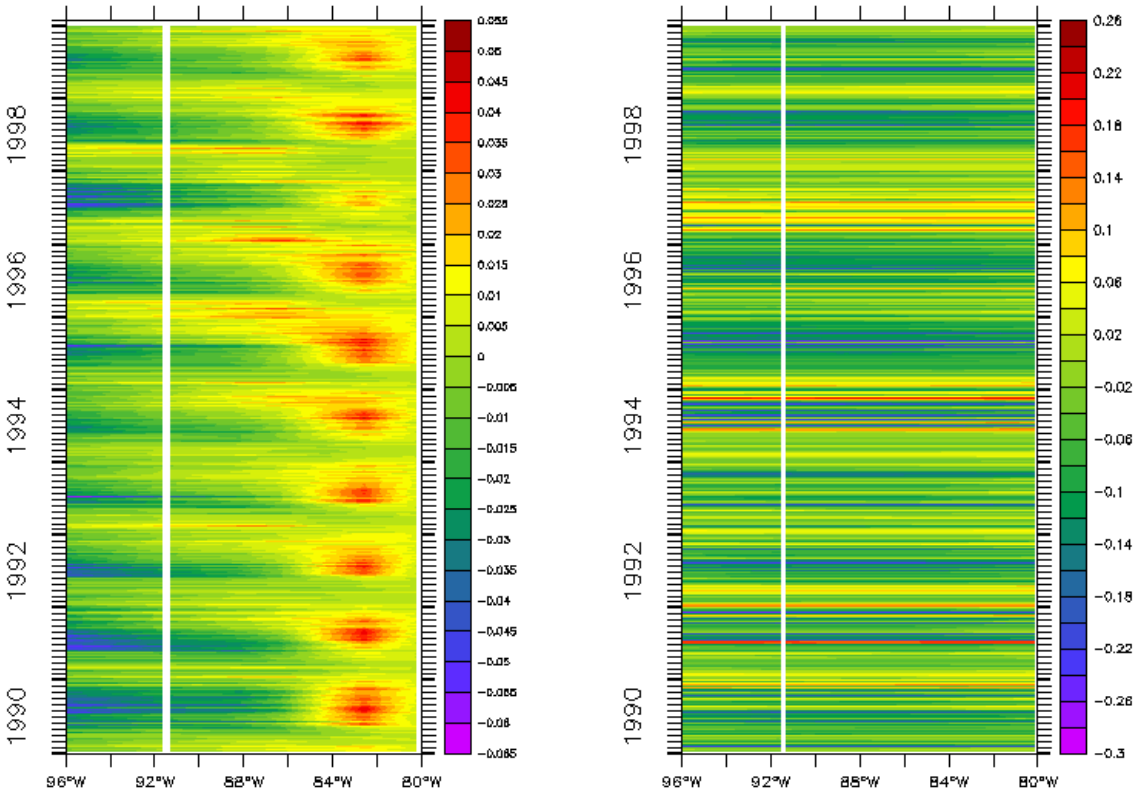

Figure 8. Time variation of zonal wind stress (N m^{-2}) and sea surface height (m) at the equator.

Moreover, during the period of the increasing SSH due to the El Niño, we can infer a deepening of the thermocline. This is because deepening of thermocline is accompanied with a rise of temperature, consequently there is an expansion of the water column, and as a result the sea level increases. Generally, there is a positive relationship between sea level and thermocline depth.

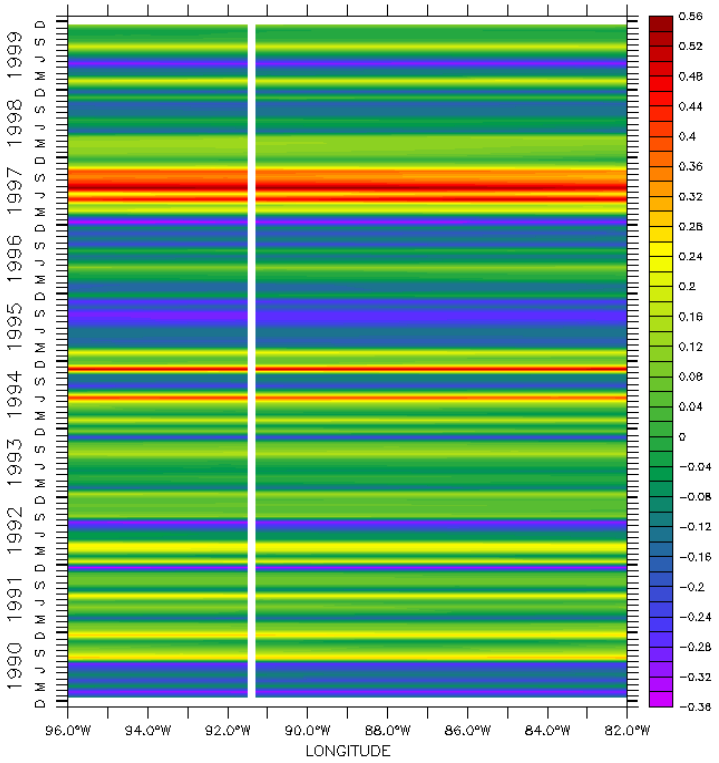

Figure 9. Time variation of SSH (m) anomalies.

3.3.3 Variation of Zonal Velocity

The modeled surface zonal velocity at the equator suggests that there is an eastward movement of currents during the first months of each year. In contrast, between July and September there is an increased westward zonal velocity that is part of the regular annual cycle in the eastern Equatorial Pacific. This occurs because the eastward pressure force is normally balanced by westward wind stress, but it is unbalanced mainly during March and April. Therefore, this pressure force accelerates the equatorial currents eastward. Figure 8 shows that there is weak activity of westward winds during the first months of the year that is accompanied by a weakness in the westward surface zonal

velocity. After July the zonal wind start to change giving an increased westward zonal wind that also allows the spread of the equatorial cold tongue.

During 1997-98 there is an increased intensity of the eastward surface zonal velocity starting in July 1997 (Figure 6), that is very unusual in that during this time one expects intensified westward zonal velocity that allows the movement from the east to the west of cold waters. Positive anomalies of eastward zonal velocities from July 1997 are detected that are stronger than occurred in 1996, an ENSO neutral. A peak of eastward movement is appreciated in March 1998. The strongest anomalies of surface zonal velocities of the 1990s occur between 1997 and 1998 (Figure 6). As we can observe, the main circulation of the region during the El Niño the cold westward south equatorial current is relaxed. We can infer that there is a contribution of the eastward advection to the increase of the SST in the eastern Tropical Pacific.

3.3.4 Variation in the Vertical Thermal Structure

Throughout the decade from 1990 to 1999 there is a clear annual cycle in the variation of temperature at 94°W and at the equator (Figure 10). Annual changes of temperature are reproduced not only at the surface but also into the upper layers of the ocean, in this case, between 50 and 100 meters. Thus, there is an increase in temperature from January to May with a peak in April of about 26°C at 40 meters of depth (Figure 10) and a decrease of temperature during August and September of about 21°C at the same depth. The variation of thermocline depth is present each year with a typical deepening during the first months of each year. The 20°C isotherm reflects the position of the thermocline in the time-longitude diagram in Figure 11.

There are two important interannual changes in the thermocline depth that occur during the El Niño events in 1992 and 1997-98. These changes affect thermocline depth to the west of the Galapagos Islands. In a normal year thermocline depth has a peak in depth of 50 meters. The position of the thermocline in years such as 1990 and 1991 is about 50 meters to the west of the Galapagos Islands. However, during the mature phase of El Niño there is a prominent deepening of the thermocline evident in 1992 with a thermocline depth of 90 meters. In addition, changes between different El Niño are apparent. For instance, in 1998 there is a deeper thermocline than in 1992. In 1992 the peak in depth reach roughly 90 meters and the peak of 1998 reach 110 meters (Figure 11).

A relevant difference between annual and interannual variability is that interannual changes involve a larger period of warming than for annual variations. In Figure 10 it is observed that El Niño 1997-98 has a deepening of thermocline that lasts for almost a full year. The El Niño of 1991-92, a moderate event, has warming that is not that much different than in 1990 and 1993. The peaks in depth of thermocline of El Niño consist of zonal redistribution of the thermocline depth over the longitudes of the domain (Figure 10).

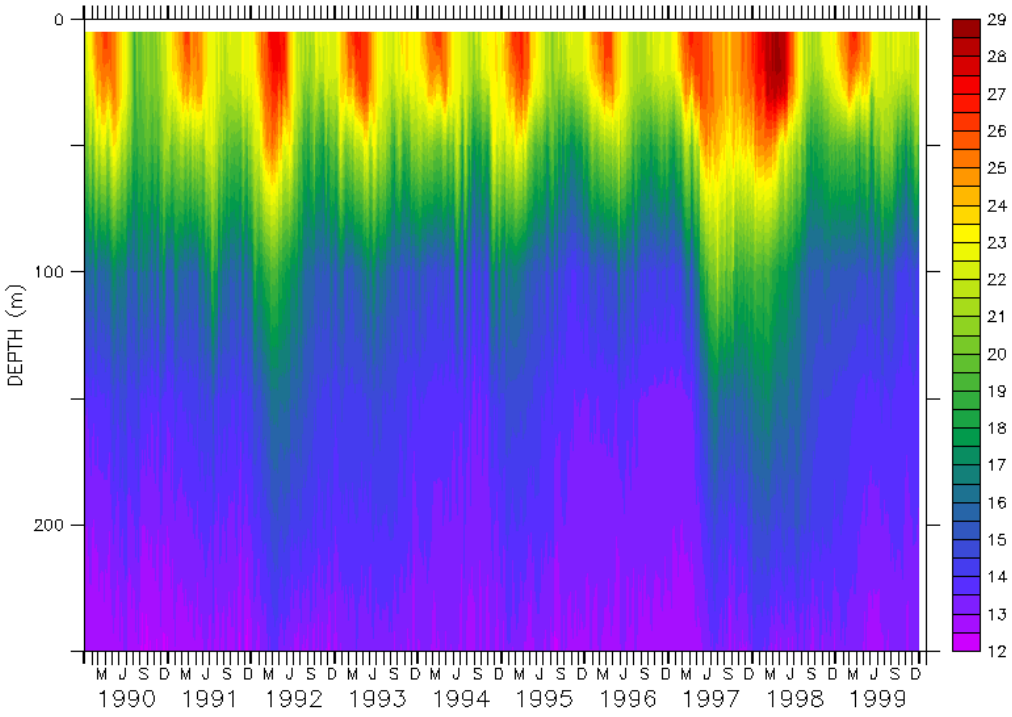

Figure 10. Time variation of temperature (°C) at 94°W at the equator.

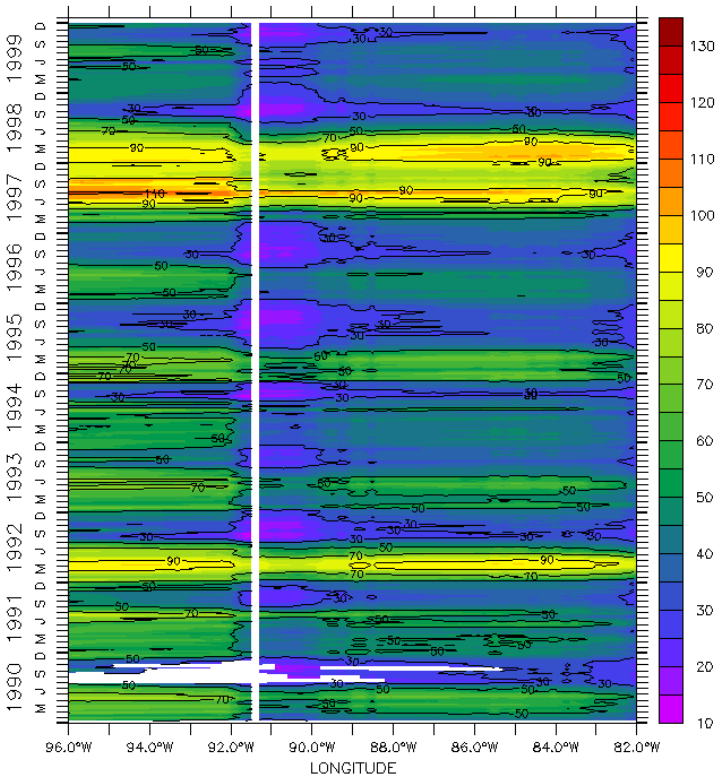

Figure 11. Time-longitude variation of the 20°C isotherm (m) at the equator.

3.4 Changes around the Galapagos Islands during El Niño of 1997-1998

3.4.1 SST and SSH Anomalies

Time averaged anomalies (from mid-December 1997 to mid-February 1998) of SST and SSH around the Galapagos Islands (from 96°W to 86°W and from 15°S to 15°N) are presented in Figure 12. The corresponding climatology used to remove the seasonal cycle was constructed from the 10 years of the model run (1990 to 1999). The El Niño of 1997-1998 had two peaks, the first one started in July 1997, and the second peak started in December 1997. Because El Niño had its mature phase starting in the beginning of December 1997, we proceed to observe the anomalies for the mature phase of El Niño. Strong positive anomalies in SST, that are a signature of the El Niño, near the Galapagos Islands mainly occur on the eastern side with a warm tongue about 4°C from 89°W to 86°W south of the equator. The western side also shows positive anomalies principally on the south-west side with positive anomalies of about 2.7°C. As we can observe in Figure 12a, there is a band of significant positive anomalous temperature between 1°N and 3°S around the Galapagos Islands.

The northeast area of the Galapagos Islands has positive anomalies of 2°C that appear similar to an extension of the anomalous thermal band along equator. During the mature phase of El Niño warming of SST reaches the eastern Tropical Pacific, therefore there is a redistribution of warm waters with the movement of the equatorial front toward the equator, and a redistribution of warm waters along the equator. Thus, it is not surprising that there are highest values of SST on the eastern side of the Galápagos Islands, considering that during the onset of El Niño events normally there are strong movements

of warm waters in the west to east direction along the equator due to the imbalance of the pressure gradient force in the ocean and the eastern trades winds.

Overall the area around Galapagos Islands (from 96°W to 86°W and from 15°S to 15°N) there is evidence of positive anomalies of sea level height (Figure 12b). There is an observable zonal gradient along the equator that runs from high to low values of positive anomalies in SSH, in the direction from west to east. Following the movement of this gradient there is a strong gradient of SSH over the southwest side of the Islands (roughly 3°S, 93°W). SSH anomalies of 0.18 meters are apparent on the western side of the Galapagos Islands, and anomalies of 0.16 meters on the eastern side (Figure 12b). This rise of sea level and the configuration of the increase can be caused by the arrival of eastward propagating equatorial Kelvin waves.

There is a noticeable increase in sea level at around 5°N and 9°W, with the highest positive anomalies of 0.23 meters in the area. Probably this area is more affected by the expansion of the water column. During the El Niño event, with warming of SST and the deepening of thermocline the water column expands and consequently the sea level rises. This observation shows a correlation between shown deepening of the thermocline in Figure 10 as compared with the same period in time (from mid-December 1997 to mid-February 1998) with a period not affected by El Niño (from mid-December 1996 to mid-February 1997).

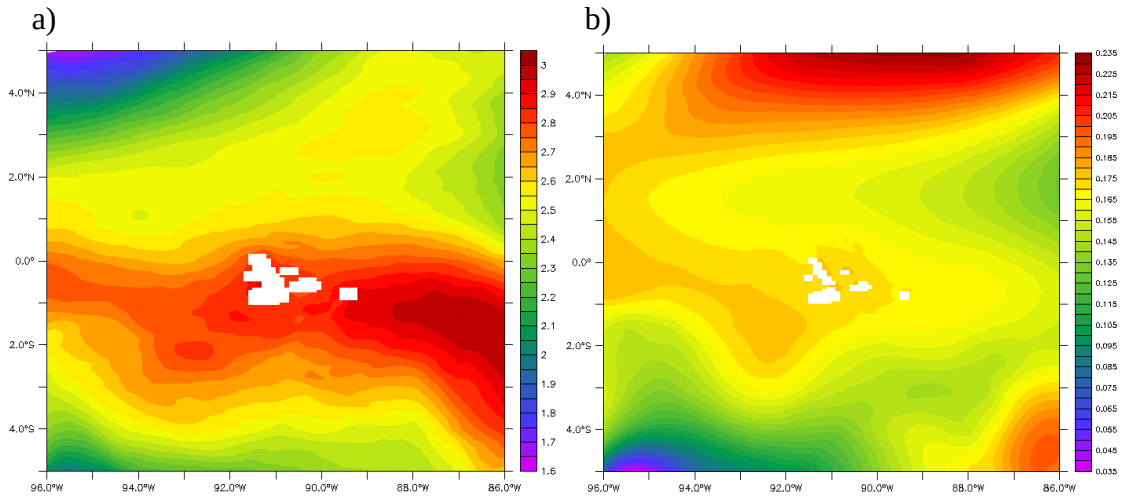

Figure 12. SST (°C) (a) and SSH (m) (b) anomalies for the period mid-December 1997 to mid-December 1998 around the Galapagos Islands.

3.4.2 Conditions during 1997-1998 in Comparison with 1996-1997

Despite the fact that El Niño 1997-98 had an early development in December 1996 in the western Equatorial Pacific, this condition was not evident on the eastern side until March and April of 1997. Figure 13 shows differences in temperature, sea surface height, horizontal and vertical velocity of between mid-December 1997 to mid-February 1998 (DJF 1997-1998) and mid-December 1996 to mid-February 1997 (DJF 1996-1997). SSH shows a tendency to increase considering differences between DJF 1997-1998 and DJF 1996-1997 that suggest strong interannual variability. Mainly, SSH differences of the two periods (DJF 1997-1998 and DJF 1996-1997) follow the sequence of anomalies for DJF 1997-1998, with evident zonal gradient of SSH from west to east (Figure 13a). Around the Galapagos Islands sea level rose 0.25 meters from DJF 1996-1997 to DJF 1997-1998.

SST shows a strong change between the two consecutive periods in the observations; that mean a rise in SST of about 3.5°C near the coast of the Galapagos Islands (Figure 13b). The rise is evident on both sides of the islands, principally over the eastern side. There is a sharp increase on the northeast side of the islands that resembles a warm tongue. This tongue arises due to the redistribution of warm waters in the eastern Tropical Pacific during the mature phase of an El Niño. Moreover, the difference of circulation between DJF 1997-1998 and DJF 1996-1997 confirms a redistribution of surface waters that according to the development of El Niño 1997-1998 during the period of comparison (December, January and February) the entire Equatorial Pacific reached hard warming SST(Figure 13b).

At a depth of 50 meters around Galapagos Islands are positive values with differences in temperature of about 5°C between DJF 1997-1998 and DJF 1996-1997. This represents an increase in temperature on a timescale comparable to the two periods for comparison (Figure 13c). We can observe that the warmest area is very close to the eastern side of the islands with a prolonged area from 90°W to 86°W along the equator. Generally, the western side of the Galapagos Islands shows an increase in temperature of 5°C. It is noticeable that an increase in the transport of waters from west to east is more evident north of 2°N and south of 1°S. Along the equator there is little change in intensity, except in the direction of the typical circulation of the area. Vertical velocity at 50 meters depth is shown in Figure 13d, where upward movement is represented by positive values and downward movement is represented by negative values. According to Figure 13d

there are not substantive changes west of the islands, except in the south where there are negative values depicting consequently downward movement of the waters.

Figure 13e shows changes in circulation and temperature from DJF 1997-1998 and DJF 1996-1997 for depths of 100 meters. Simulated temperature from ROMS shows an increase in the temperature at 100 meters depth mainly west of the Galapagos Islands at 92°W at the equator. This increase is associated with a deepening of the thermocline. Temperature around the Galapagos Islands reveals that the transport of water on the northeast and the warm tongue that are apparent at the surface and at 50 meters depth corresponds to redistribution of waters near the surface. On the other hand, the transport from west to east at the equator occurs at deeper layers. The difference in circulation from DJF 1997-1998 and DJF 1996-1997 shows that there is a continuous transport from west to east at 100 meters depth between 2°N and 2°S. The vertical velocity at this depth (100 meters) shows noticeable downwelling west of the Galapagos Islands, and to the north and south of the islands with the negative values (see Figure 13f). These values reinforce the fact that upwelling is depleted during El Niño. Principally, eastward transport of warm waters over the upper layers reduces the possibility of upwelling to the west of the Galapagos Islands due to the topography.

At 250 meters depth there is not a noticeable difference between DJF 1997-1998 and DJF 1996-1997 (Figure 13g). The increase in temperature near the Galapagos Islands only reaches 0.75°C. the highest difference is roughly 1.85 °C in the northwest area of the islands at 5°N. Here we demonstrate that the warming of temperature in the vertical only reaches the first upper layers of the ocean at the eastern Equatorial Pacific. Recall that

Figure 1 shows that the TAO buoys depict a deepening of the thermocline to 140 meters. Despite the bias in the deepening of the thermocline in ROMS, at 250 meters the influence of the deepening of the thermocline is relatively weak. Vertical velocity at 250 meter depth also doesn't have substantial changes (Figure 13h).

a) SSH differences at the surface. b) SST and U,V differences at the surface.

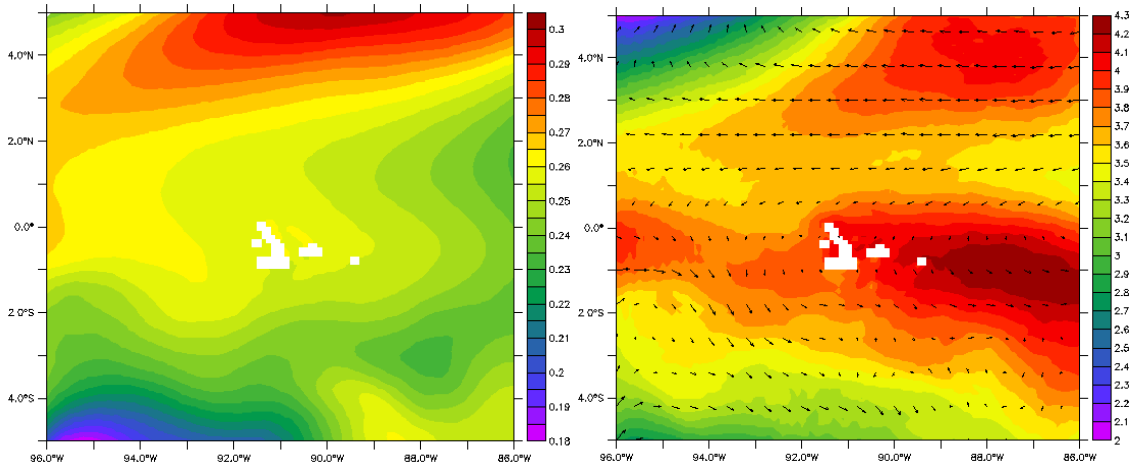

Figure 13. Differences in SSH (m) , SST (°C), temperature in depth (T), horizontal (U,V) and vertical velocity (W) (m s^{-1}) between mid-December 1997 to mid-February 1998 (DJF 1997-1998) and mid-December 1996 to mid-February 1997 (DJF 1996-1997). Red and yellow colors represent upward movements in vertical velocity (W), green and blue colors represent downward movements.

c) T and U,V differences at 50 m depth. d) W differences at 50 m depth.

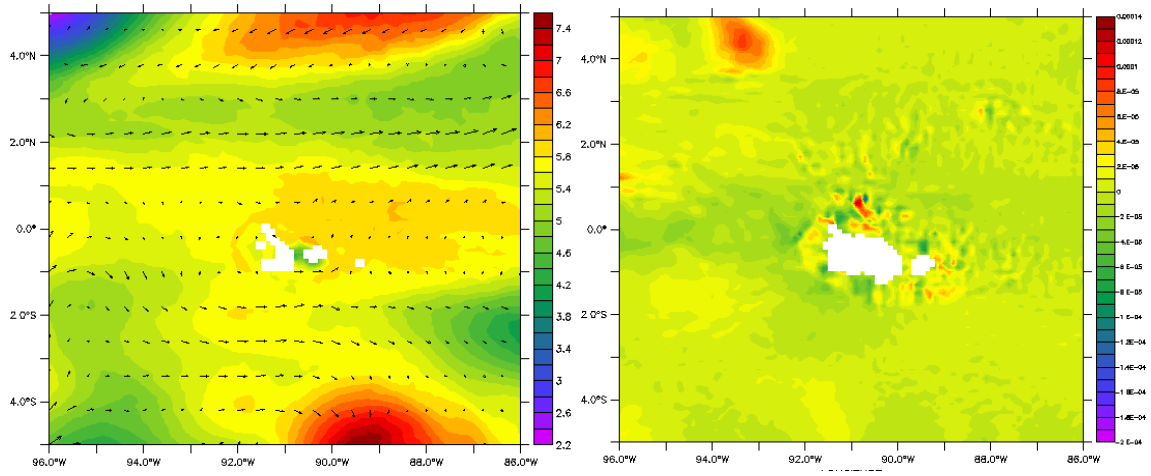

e) T and U,V differences at 100 m depth. f) W differences at 100 m depth.

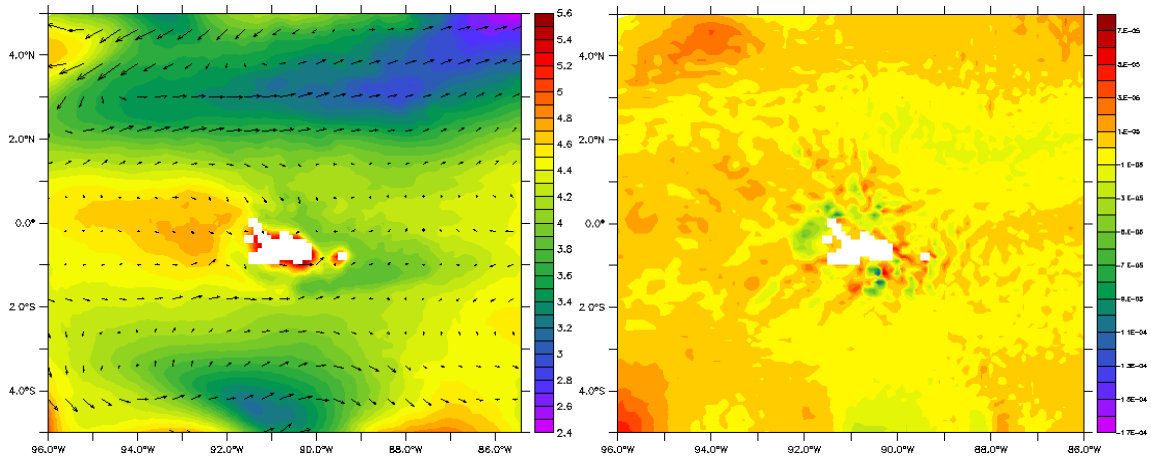

g) T and U,V differences at 250 m depth. h) W differences at 250 m depth.

Figure 13. Continued.

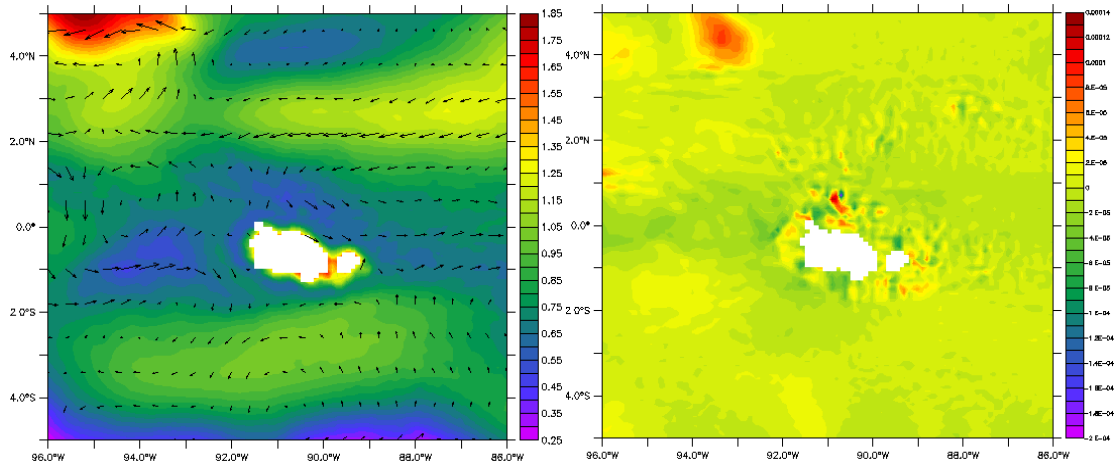

Figure 13. Continued.

CHAPTER IV

SUMMARY AND CONCLUSIONS

A high resolution ocean model (ROMS) is used to explore interannual variability in the Eastern Tropical Pacific. The model has an average resolution of 0.1° in the horizontal and covers the eastern Tropical Pacific Ocean. An experiment run from 1990 to 1999 is used to explore the mean conditions and interannual variability during this period.

A comparison of the results with observational data from a buoy that is part of the Tropical Atmosphere Ocean (TAO) project located at 95°W at the equator shows that the modeled sea surface temperature is able to capture the main features of the annual cycle; with a warm phase during February through May of each year, and a cold phase during August and September. Interannual variability between 1996 and the middle of 1998 demonstrates the basic change from a regular year and El Niño year with a peak warming in SST during DJF at 1998. The model captures the main features of variability of both seasonal cycle and of interannual variability. In magnitude of SST there is a general bias of about 1 to 1.5°C in the representation of regular cold episodes of a year and the development of an El Niño. However, the modeled temperature follows the main sequence of events in comparison with the TAO buoy data.

The vertical structure of temperature from ROMS agrees with recorded TAO buoy data with a good representation of the interannual variability. Warm and cold episodes in the subsurface in ROMS captures the same general features for the seasonal cycle as well.

To explore interannual changes we compare the variation in thermocline depth of 1997 and 1998 with the years of 1995 and 1996. Modeled temperatures present a vertical distribution and stratification that represents the observations fairly well. However, there is a bias such that the model underestimates the depth of the thermocline during the second peak of the El Niño of 1997-1998. Overalls the model follows the relevant evolution of the events that allow us to use this information to analyze the interannual variability.

Mean conditions in surface and vertical structure from the ROMS output present the expected features and behavior of the Eastern Equatorial Pacific. Therefore, the model was able to represent the most relevant characteristics of the domain of study. In particular the cold tongue is clearly defined by SST along the equatorial coastal upwelling, with warm temperatures north of the equator as the equatorial front. The model also captures the Costa Rica Dome a feature particular to the eastern tropical Pacific Ocean. The main surface ocean circulation of the model allows us to document the circulation of the area, which includes the SEC, NECC, and the NECC. The main thermal vertical structure from the upper layers form west to east on the equator demonstrated by the shallow thermocline and the strong thermal gradient that is an important characteristic of the Eastern Equatorial Pacific. The subsurface main ocean circulation of ROMS presented by a cross section of the western side of the Galapagos Islands agree with the documental circulation of the area, in which we identify the EUC, NECC, and the NEC. These currents are governed by the geostrophic balance and the gradient of the isotherms just over the NECC considering a meridional section west of the Galapagos Islands.

The results of the run for the period from 1990 to 1999 chose for this analysis shows evidence that El Niño events represent the most important features in the interannual variability at the Eastern Equatorial Pacific. Comparing the years 1997-1998 and 1991-1992 with the regular years reveals that there are prominent changes mainly in the distribution in time of SST. For instance we found that the warm phase of El Niño 1997-1998 has an extended period of anomalous warming in comparison with years with a regular behavior at the Eastern Equatorial Pacific such as 1995 and 1996 where the warming of SST is locked only to the annual cycle. In addition, these changes were also found in the vertical distribution of temperature with a deepening of the thermocline with a prolonged period of anomalous warming. Therefore, we can assert that one of the most interesting features of El Niño is the continued warming at the surface and subsurface layers that contrast with the annual cycle with shorter periods that agree with the theory of El Niño. In addition, it was observed that warming was restricted to the upper layers to a depth of about 120 meters.

An anomalous SSH was detected during the occurrence of El Niño that appears mainly during the first peak of the El Niño of 1997-1998. The rise of SSH has a positive relationship with the deepening of the thermocline, because of the relationship between betaken sea level height and thermocline depth due to the increase of temperature and consequently the expansion of the water column.

Changes around the Galapagos Islands during the El Niño of 1997-1998 were evident as we could determine by analyzing the anomalies on the surface related to SST and SSH, and with a comparison using the difference between conditions during the

second peak of El Niño in 1997-1998 and a period before the El Niño, 1996-1997. This study is focused on the surroundings of the Galapagos Islands where we can determine that there was a strong change along the equator represented by a band of warm waters with the highest anomaly of SST on the western side of the Islands. We might infer that this feature corresponds to the redistribution of warm waters during the mature phase of an El Niño, this assertion is supported by the presentation of the redistribution of surface waters through the difference of both 1997-1998 years and 1996-1997 years. We also found an interesting eastward sloping of the SSH with the anomalies forming high to low values on the eastern side of the Galapagos Islands.

We observed that the zonal band of warm waters around the Galapagos Islands during the El Niño 1997-1998 is deeper on the western side than on the eastern side. The eastern side is controlled by warm waters from the warm tongue formed on this side, while the western side has warming in deeper waters because of the advection from west to east of warm waters in earlier phases of the development of El Niño. At a depth of 100 meters warming on the western side is stronger in comparison with the eastern side by more than 1°C.

Moreover, ocean circulation in the upper layers up to a depth of 250 meters showed us the redistribution of waters from west to east and vice versa. This redistribution is most noticeable at a depth of 100 meters. In addition, vertical velocity gives us an idea of the upward and downward movement of waters and shows a noticeable downward movement on the western side of the Galapagos Islands at depths of 100 meters, at the same time we had the highest difference of SST during DJF 1997-1998 in comparison with DJF 1996-

1997. A weaker difference in vertical velocity with negative values was observed at 50 meters depth on the same side-which side of the Islands. These results are expected based on the theory of reduced upwelling during an El Niño event. However, we cannot assert a relationship of temperature and upwelling for this period of analysis.

REFERENCES

Bjerknes, J. (1969), Atmospheric teleconnections from the equatorial pacific 1, Mon.Weather Rev., 97(3), 163-172.

Carton, J.A., and B.S. Giese (2008), A reanalysis of ocean climate using Simple Ocean Data Assimilation (SODA), Mon.Weather Rev., 136(8), 2999-3017.

Chang, P. (1993), Seasonal cycle of sea surface temperature and mixed layer heat budget in the tropical Pacific Ocean, Geophys.Res.Lett., 20(19), 2079-2082.

Chapman, D.C. (1985), Numerical treatment of cross-shelf open boundaries in a barotropic coastal ocean model, J.Phys.Oceanogr., 15(8), 1060-1075.

Colas, F., X. Capet, J. McWilliams and A. Shchepetkin (2008), 1997–1998 El Niño off Peru: A numerical study, Prog.Oceanogr., 79(2), 138-155.

Compo, G.P., J.S. Whitaker and P.D. Sardeshmukh (2006), Feasibility of a 100-year reanalysis using only surface pressure data, Bull.Am.Meteorol.Soc., 87(2), 175-190.

Compo, G.P., J.S. Whitaker, P.D. Sardeshmukh, N. Matsui, R. Allan, X. Yin, B. Gleason, R. Vose, G. Rutledge and P. Bessemoulin (2011), The twentieth century reanalysis project, Q.J.R.Meteorol.Soc., 137(654), 1-28.

Dewitte, B., J. Vazquez-Cuervo, K. Goubanova, S. Illig, K. Takahashi, G. Cambon, S. Purca, D. Correa, D. Gutierrez and A. Sifeddine (2012), Change in El Niño flavours over 1958–2008: Implications for the long-term trend of the upwelling off Peru, Deep Sea Research Part II: Topical Studies in Oceanography., 77, 143-156.

Flather, R. (1976), {A tidal model of the northwest European continental shelf}, Mem.Soc.R.Sci.Liege., 10(6), 141-164.

Giese, B.S., and J.A. Carton (1999), Interannual and decadal variability in the tropical and midlatitude Pacific Ocean, J.Clim., 12(12), 3402-3418.

Giese, B.S., and S. Ray (2011), El Niño variability in simple ocean data assimilation (SODA), 1871–2008, Journal of Geophysical Research: Oceans (1978–2012)., 116(C2).

Haidvogel, D.B., H. Arango, W.P. Budgell, B.D. Cornuelle, E. Curchitser, E. Di Lorenzo, K. Fennel, W.R. Geyer, A.J. Hermann and L. Lanerolle (2008), Ocean forecasting in terrain-following coordinates: Formulation and skill assessment of the

Regional Ocean Modeling System, Journal of Computational Physics., 227(7), 3595-3624.

Haidvogel, D.B., H.G. Arango, K. Hedstrom, A. Beckmann, P. Malanotte-Rizzoli and A.F. Shchepetkin (2000), Model evaluation experiments in the North Atlantic Basin: simulations in nonlinear terrain-following coordinates, Dyn.Atmos.Oceans., 32(3), 239-281.

Jin, F., and J.D. Neelin (1993), Modes of interannual tropical ocean-atmosphere interaction-A unified view. Part I: Numerical results, J.Atmos.Sci., 50(21), 3477-3503.

Jones, P.W. (1999), First-and second-order conservative remapping schemes for grids in spherical coordinates, Mon.Weather Rev., 127(9), 2204-2210.

Kessler, W.S. (2006), The circulation of the eastern tropical Pacific: A review, Prog.Oceanogr., 69(2), 181-217.

Kruk, M.C., K.R. Knapp and D.H. Levinson (2010), A technique for combining global tropical cyclone best track data, J.Atmos.Ocean.Technol., 27(4), 680-692.

Lemarié, F., J. Kurian, A.F. Shchepetkin, M. Jeroen Molemaker, F. Colas and J.C. McWilliams (2012), Are there inescapable issues prohibiting the use of terrain-following coordinates in climate models?, Ocean Modelling., 42, 57-79.

Li, T., and S.G.H. Philander (1996), On the annual cycle of the eastern equatorial Pacific, J.Clim., 9(12), 2986-2998.

Marchesiello, P., J.C. McWilliams and A. Shchepetkin (2001), Open boundary conditions for long-term integration of regional oceanic models, Ocean modelling., 3(1), 1-20.

Mellor, G.L., and T. Yamada (1982), Development of a turbulence closure model for geophysical fluid problems, Rev.Geophys., 20(4), 851-875.

Montes, I., F. Colas, X. Capet and W. Schneider (2010), On the pathways of the equatorial subsurface currents in the eastern equatorial Pacific and their contributions to the Peru-Chile Undercurrent, Journal of Geophysical Research: Oceans (1978–2012)., 115(C9).

Penven, P., V. Echevin, J. Pasapera, F. Colas and J. Tam (2005), Average circulation, seasonal cycle, and mesoscale dynamics of the Peru Current System: A modeling approach, Journal of Geophysical Research: Oceans (1978–2012)., 110(C10).

Philander, S.G.H., D. Philander, G. Gu, T. Lambert, D. Li, N. Halpern, R.C. Lau and Pacanowski (1996), Why the ITCZ Is Mostly North of the Equator, J.Clim., 9(12), 2958-2972, doi: 10.1175/1520-0442(1996)009<2958:WTIIMN>2.0.CO;2.

Philander, S.G.H., W.J. Philander, A.D. Hurlin and Seigel (1987), Simulation of the Seasonal Cycle of the Tropical Pacific Ocean, J.Phys.Oceanogr., 17(11), 1986-2002, doi: 10.1175/1520-0485(1987)017<1986:SOTSCO>2.0.CO;2.

Philander, S. (1981), The response of equatorial oceans to a relaxation of the trade winds, J.Phys.Oceanogr., 11(2), 176-189.

Phillips, N.A. (1957), A coordinate system having some special advantages for numerical forecasting, J.Meteorol., 14(2), 184-185.

Rasmusson, E.M., and T.H. Carpenter (1982), Variations in tropical sea surface temperature and surface wind fields associated with the Southern Oscillation/El Niño, Mon.Weather Rev., 110(5), 354-384.

Russon, T., A. Tudhope, G. Hegerl, A. Schurer and M. Collins (2014), Assessing the significance of changes in ENSO amplitude using variance metrics, J.Clim.(2014).

Sarachik, E.S., and M.A. Cane (2010), The El Nino-southern oscillation phenomenon, Cambridge University Press.

Shchepetkin, A.F., and J.C. McWilliams (2005), The regional oceanic modeling system (ROMS): a split-explicit, free-surface, topography-following-coordinate oceanic model, Ocean Modelling., 9(4), 347-404.

Shchepetkin, A.F., and J.C. McWilliams (2003), A method for computing horizontal pressure-gradient force in an oceanic model with a nonaligned vertical coordinate, Journal of Geophysical Research: Oceans (1978–2012)., 108(C3).

Smith, R., J. Dukowicz and R. Malone (1992), Parallel ocean general circulation modeling, Physica D., 60(1), 38-61.

Song, Y., and D. Haidvogel (1994), A semi-implicit ocean circulation model using a generalized topography-following coordinate system, Journal of Computational Physics., 115(1), 228-244.

Tziperman, E., S.E. Zebiak and M.A. Cane (1997), Mechanisms of seasonal-ENSO interaction, J.Atmos.Sci., 54(1), 61-71.

Wang, B. (1995), Interdecadal changes in El Nino onset in the last four decades, J.Clim., 8(2), 267-285.

Wang, C., and P.C. Fiedler (2006), ENSO variability and the eastern tropical Pacific: a review, Prog.Oceanogr., 69(2), 239-266.

Wang, C., and R.H. Weisberg (2000), The 1997-98 El Niño evolution relative to previous El Niño events, J.Clim., 13(2), 488-501.

Whitaker, J.S., G.P. Compo, X. Wei and T.M. Hamill (2004), Reanalysis without radiosondes using ensemble data assimilation, Mon.Weather Rev., 132(5), 1190-1200.

Woodruff, S.D., S.J. Worley, S.J. Lubker, Z. Ji, J. Eric Freeman, D.I. Berry, P. Brohan, E.C. Kent, R.W. Reynolds and S.R. Smith (2011), ICOADS Release 2.5: extensions and enhancements to the surface marine meteorological archive, Int.J.Climatol., 31(7), 951-967.

Wyrtki, K. (1975), El Niño-The dynamic response of the equatorial Pacific oceanto atmospheric forcing, J.Phys.Oceanogr., 5(4), 572-584.

Xie, S. (1994), On the genesis of the equatorial annual cycle, J.Clim., 7(12), 2008-2013.

Yin, X., B. Gleason, G. Compo, N. Matsui and R. Vose (2008), The International Surface Pressure Databank (ISPD) land component version 2.2, National Climatic Data Center: Asheville, NC.Available from ftp://ftp.ncdc.noaa.gov/pub/data/ispd/doc/ISPD2., 2.